ELSEVIER

International Journal of Heat and Fluid Flow 23 (2002) 519–529

International Journal of HEAT AND FLUID FLOW

www.elsevier.com/locate/ijhff

Laminar natural convection in a vertical isothermal channel with symmetric surface-mounted rectangular ribs

Gilles Desrayaud [a,*], Alberto Fichera [b]

[a] *LETEM Laboratory, INSSET, Université de Picardie Jules Verne, 48 rue Raspail BP 422, 02109 Saint-Quentin Cedex, France*
[b] *Istituto Fisica Tecnica, Università di Catania, Viale A. Doria 6, 95125 Catania, Italy*

Received 17 September 2001; accepted 11 December 2001

Abstract

In this paper, a numerical investigation of laminar natural convective flows in a vertical isothermal channel with two rectangular ribs, symmetrically located on each wall, is carried out. The governing elliptic equations are solved in a two-dimensional domain using a control volume method and the SIMPLER algorithm for the velocity–pressure coupling is employed. Special emphasis is given in the systematic analysis to detail the effects of the location of the isothermal ribs on the flow structure and isotherms pattern. The profiles of the local Nusselt number are presented for three different locations of the obstructions, near the inlet, at the center and near the outlet of the channel. The influence of the rib conductivity is also considered, the ribs being either perfectly conducting or adiabatic. The variations in the mean Nusselt number and inlet flow rate versus the channel Rayleigh number are investigated. Finally, for centered ribs extra computations are performed for various sizes (width and length) of the ribs and for two aspect ratios to demonstrated the significant effects on the flow and heat transfer characteristics.

Keywords: Isothermal channel; Natural convection; Rectangular rib; Control volume method

1. Introduction

In the literature, a large number of theoretical and experimental investigations are reported on natural convection in vertical channels. The seminal work in this field is that of Elenbaas (1942), in which an experimental relation between the mean Nusselt number and the channel Rayleigh number was proposed, and this correlation is now often compared with numerical and analytical results in vertical channels. Bar-Cohen and Rohsenow (1984) also presented correlations, which extend from the fully developed regime to the single plate regime for various kinds of boundary conditions. As regards the numerical approach, the first study was that of Bodoia and Osterle (1962). They solved a parabolic form of the governing equations in a vertical isothermal channel and their results are in good agreement with the experimental correlation of Elenbaas (1942). Subsequently, Kettleborough (1972) and Nakamura et al. (1982) introduced the full elliptical form of the governing equations of natural convection in a vertical channel, which enables flow recirculation to be taken into account. As the literature on this problem is very extensive, only a small fraction has been cited here.

It can be observed that although natural convection in vertical smooth channels has been studied extensively, the problem of natural convection with large-scale roughness elements has been less frequently reported in the literature, even though it is encountered in several technological applications. Often, the purpose of protuberances is to enhance heat transfer by providing additional surface area as in exchanger devices, which can lead to the development of a variety of unconventional internal flow passages. In some circumstances, such roughness elements occur naturally as in chimneys or in electronic circuit boards and natural convective flow may be significantly altered by roughness elements mounted on the surfaces.

Habchi and Acharya (1986) numerically investigated the laminar mixed convection of air in a vertical channel with a single rectangular rib. They demonstrated that

* Corresponding author. Tel.: +33-3-23-62-89-37; fax: +33-3-23-62-89-35.
E-mail address: gilles.desrayaud@insset.u-picardie.fr (G. Desrayaud).

0142-727X/02/$ - see front matter
PII: S0142-727X(02)00136-4

Nomenclature

a	inter-rib spacing ($a = b - 2w$)
A	aspect ratio of the channel ($A = L/b$)
b	channel width
g	gravitational acceleration
h	rib length
h_{cv}	local wall heat transfer coefficient
$\overline{h}_{cv}$	mean wall heat transfer coefficient
k	thermal conductivity of the fluid
L	channel height
L_1	rib location from channel inlet
Nu	local Nusselt number
$\overline{Nu}$	mean Nusselt number
p	static pressure
P_m	dimensionless motion pressure
Pr	Prandtl number ($Pr = \nu/\alpha$)
Q	dimensionless mass flow rate
Ra	Rayleigh number ($Ra = g\beta\Delta Tb^3/\alpha\nu$)
Ra^*	channel Rayleigh number ($Ra^* = Ra/A$)
T_0	ambient temperature
T_w	wall temperature
X, Y	dimensionless coordinates
U, V	dimensionless velocity components in X and Y directions
w	rib width

Greeks

α	thermal diffusivity
β	volumetric coefficient of expansion
θ	dimensionless temperature ($\theta = (T - T_0)/\Delta T$)
ρ	density of the fluid
ν	kinematic viscosity of the fluid
ΔT	temperature difference ($\Delta T = T_w - T_0$)

Subscript

w	at wall

Superscript

$*$	dimensionless geometrical variables

for a symmetrically or asymmetrically heated channel, the mean Nusselt numbers are smaller than the corresponding smooth channel Nusselt numbers, i.e. for an unobstructed channel. Hung and Shiau (1988) conducted experimental work in a vertical heated channel with a single rectangular rib under asymmetric isoflux heating and found that the channel spacing has no significant effect on mean heat transfer characteristics if convective heat flux is maintained constant. In the downstream region of the rib, the flow was turbulent. Said and Krane (1990) performed a numerical and experimental investigation of natural convection in a vertical channel with a single semi-circular obstacle. They showed that the location of the rib along the wall affects the rate of heat transfer. Owing to the presence of the obstacle, the reduction of the mean Nusselt number can reach 40% (respectively 5%) for low channel Rayleigh number, i.e. $Ra^* = 10$ (respectively, $Ra^* = 10^4$). Natural convection from a vertical isothermal surface with repeated ribs or steps has been experimentally studied by Bhavnani and Bergles (1990). They demonstrated that stepped surfaces helped improve the heat transfer while ribbed surfaces resulted in degraded heat transfer performance (compared to that of a plain plate of equal projected area). In another recent study, Tanda (1997) performed an experimental study of natural convection inside vertical channels formed by a heated ribbed surface and an opposing unheated smooth surface. He found that the presence of ribs worsens heat transfer performance due to inactive regions just upstream and downstream of each protrusion. Tanda concluded that adding ribs for the purpose of heat transfer augmentation is useless for natural convection and that care must be taken in thermal design when large-scale roughness elements occur naturally, especially in narrow passages. Kwak and Song (1998) studied experimentally and numerically the natural convection from a grooved plate with different sizes of the grooves. They also demonstrated that the total heat transfer rate from the grooved surface can be smaller than that of a flat plate in spite of the increased surface area.

Recently, Hadjadj and El Kyal (1999) studied numerically laminar natural convective flow of various fluids in a vertical concentric annulus with two sinusoidal protuberances. These symmetrically surface-mounted elements are located at the center of the external and internal surfaces of the inner and outer cylinders. The protuberance amplitude has a major influence on the flow structure and isotherm pattern, and leads to an increase in heat transfer rates at the obstructions. This result seems to be contradictory to the conclusion found by Habchi and Acharya (1986) and Said and Krane (1990) for a single obstacle and Kwak and Song (1998) and Bhavnani and Bergles (1990) for arrays of obstacles. It should be noted that Hadjadj and El Kyal (1999) in their numerical study used unconventional inlet and outlet boundary conditions, i.e. zero streamwise gradient for all of the variables (velocity, pressure and temperature) while Said and Krane experimentally corroborated their numerical results.

In this paper, some results of a systematic study of a vertical isothermal channel with a single isothermal or adiabatic rectangular rib on both walls are presented, the flow being considered steady and laminar. Numeri-

cal simulations have been conducted to determine the heat transfer and the flow rates for unobstructed and obstructed channels. The distance of the ribs from the leading edge of the channel is one of the key geometrical parameters. The main purpose of this study is to establish the effect produced by the location of rectangular ribs on the heat transfer characteristics of symmetrically heated vertical channels for a fixed geometry of the ribs. The influences of parametric changes in the obstacle geometry as well as the effects of aspect ratio upon the flow and heat transfer are also examined. These results document the dependence of the mass flow rate and mean Nusselt number on the governing parameters.

2. Mathematical model

In the proposed study, rectangular ribs of length h and width w are placed on both walls inside a vertical two-dimensional channel formed by two isothermal plates of length L separated by a distance b (Fig. 1). The obstacles are located at a distance L_1 downstream of the channel inlet. The local distance x along the channel is measured from the leading edge of the left plate of the channel.

The flow is considered steady, laminar and incompressible and the Boussinesq approximation has been applied. The thermo-physical quantities are all assumed to be constant except for the density in the buoyancy force. Natural convection in a vertical channel has usually been solved numerically, adopting a parabolic scheme. It is not possible to use such a marching scheme to obtain a solution for the vertical obstructed channel since the presence of recirculating flows makes the problem elliptical.

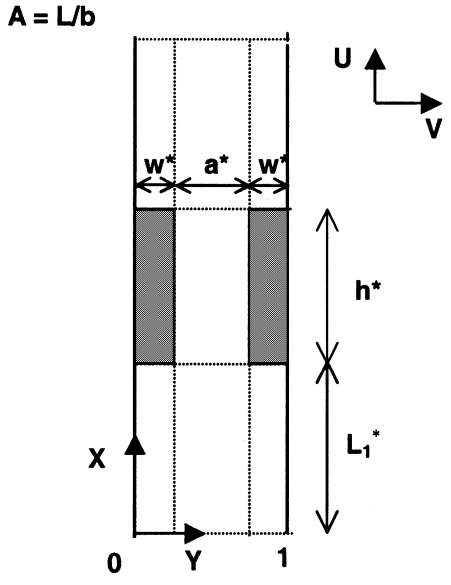

Fig. 1. Geometry of the obstructed channel.

For this reason, an elliptical numerical scheme has been used to solve the governing equations. With these assumptions, the dimensionless governing equations can be written as

$$\frac{\partial U}{\partial X}+\frac{\partial V}{\partial Y}=0 \tag{1}$$

$$U\frac{\partial U}{\partial X}+V\frac{\partial U}{\partial Y}=-\frac{\partial P_{\mathrm{m}}}{\partial X}+Pr\left(\frac{\partial^2 U}{\partial X^2}+\frac{\partial^2 U}{\partial Y^2}\right)+RaPr\theta \tag{2a}$$

$$U\frac{\partial V}{\partial X}+V\frac{\partial V}{\partial Y}=-\frac{\partial P_{\mathrm{m}}}{\partial Y}+Pr\left(\frac{\partial^2 V}{\partial X^2}+\frac{\partial^2 V}{\partial Y^2}\right) \tag{2b}$$

$$U\frac{\partial \theta}{\partial X}+V\frac{\partial \theta}{\partial Y}=\left(\frac{\partial^2 \theta}{\partial X^2}+\frac{\partial^2 \theta}{\partial Y^2}\right) \tag{3}$$

Referring to Fig. 1, the dimensionless variables are:

$$X=\frac{x}{b},\quad Y=\frac{y}{b},\quad U=\frac{ub}{\alpha},\quad V=\frac{vb}{\alpha},\quad \theta=\frac{T-T_0}{T_{\mathrm{W}}-T_0}$$

$$P_{\mathrm{m}}=\frac{(p+\rho gx)b^2}{\rho\alpha^2},\quad Ra=\frac{g\beta\Delta Tb^3}{\alpha v},\quad Pr=\frac{v}{\alpha}$$

Using the hydrostatic fundamental relation for the atmospheric pressure on the outside of the channel, the motion pressure P_{m} is also given by the difference between the pressure inside the channel and the pressure outside at the same elevation. The governing parameters which appear in the equations are the Rayleigh number based on the width of the channel and the Prandtl number. The working fluid being air, in what follows the Prandtl number is taken to be equal to 0.71.

The problem considered is a boundary value problem so it needs inlet and outlet information. Thus, the boundary conditions for Eqs. (1)–(3) are the following:

$0\leqslant Y\leqslant 1$ and $X=0$:

$$\frac{\partial U}{\partial X}=0,\quad V=0;\quad \theta=0,\quad P_{\mathrm{m}}=-\frac{Q^2}{2}\quad \text{(Inlet)} \tag{4}$$

$0\leqslant Y\leqslant 1$ and $X=A$:

$$\frac{\partial \theta}{\partial X}=\frac{\partial U}{\partial X}=\frac{\partial V}{\partial X}=0,\quad P_{\mathrm{m}}=0\quad \text{(Outlet)} \tag{5}$$

$0\leqslant X\leqslant A$ and $Y=0;1$:

$$\theta=1,\quad U=V=0,\quad \frac{\partial P_{\mathrm{m}}}{\partial Y}=0\quad \text{(Left and right walls)} \tag{6}$$

The mass flow rate is calculated at the entrance of the channel as, $Q=\int_0^1 U\,\mathrm{d}Y$.

For reasonably high values of Ra^* ($\geqslant 100$), any region outside the channel can be neglected, upstream thermal diffusion through the inlet section being negligible. Thus, because the fluid is not pre-heated before entering, the computational domain can be restricted to

the space between the plates. The fluid is assumed to enter into the channel at ambient temperature T_0 and the mass flow rate, Q, depends on the square root of the difference between the ambient pressure and the pressure at the inlet cell as confirmed by the Bernoulli equation. The walls are maintained at uniform temperature T_w. Finally, at the upper boundary, the streamwise variations of the velocity components and temperature are neglected while the pressure is assumed to be equal to the ambient pressure. The fluid entering through the outlet section of the channel (with downward velocity) is at the ambient temperature. This is an approximation because the outside environment is not able to provide totally fresh air to the recirculation. Zamora and Hernandez (1997) have shown, for Boussinesq and non-Boussinesq fluid flows, that these types of boundary condition (Eq. (5)) are able to capture outlet recirculation flows. Recently, Marcondes and Maliska (1999) numerically demonstrated the importance of the inlet pressure boundary condition for properly capturing outlet flow reversal adjacent to the adiabatic wall in an asymmetrically heated channel. They showed that using $P_m = 0$ instead of $P_m = -0.5Q^2$, has no noticeable influence on the mean Nusselt number but substantially increases the mass flow rate and inhibits the occurrence of outlet flow reversal. Furthermore, good comparison of flow reversal was found with the experimental work of Sparrow et al. (1984), which gives confidence in such outlet boundary conditions.

To evaluate the heat transfer *at the wall surface* of the channel, the local and mean Nusselt numbers based on the channel width are defined as follows:

$$Nu = \frac{h_{cv} b}{k} = \left(\frac{-k \frac{\partial T}{\partial y}}{k \frac{\Delta T}{b}} \right)_{y=0} = \left(-\frac{\partial \theta}{\partial Y} \right)_{Y=0} \tag{7}$$

$$\overline{Nu} = \frac{\overline{h}_{cv} b}{k} = -\frac{1}{A} \int_0^A \left(\frac{\partial \theta}{\partial Y} \right)_{Y=0} dX \tag{8}$$

It should be noted that the heat flux extracted by conduction at the base of the rib is the heat flux convected by the fluid flow from the three exposed faces of the rib. By analogy and using the 'conductive' expression of Eq. (7) (third term), a Nusselt number has been defined at the substrate–rib interface, which is also representative of the convective heat flux extracted by the rib.

The governing equations reported above are discretized on a staggered, non-uniform Cartesian grid using a finite-volume procedure with a central differencing scheme for the convective terms. The SIMPLER algorithm is employed for the velocity–pressure coupling (Patankar, 1980). The momentum and energy equations are cast in transient form and the time integration is performed using an ADI scheme until a steady final state is obtained. Under-relaxation parameters are used for velocities and temperatures to control the advancement of the solution field. The numerical code has been extensively validated against benchmark problems to check its validity.

Table 1
Grid-sensitivity test, $Ra^* = 2 \times 10^4$, $Pr = 0.71$, $w^* = 0.3$, $h^* = 1$, $A = 5$

Y-direction	X-direction	Ψ_{max}	Q	$\overline{Nu}$
32 (11, 10, 11)	102 (40, 30, 32)	135.99	133.32	5.75
42 (11, 20, 11)	102 (40, 30, 32)	150.23	147.21	5.95
42 (11, 20, 11)	122 (50, 30, 42)	151.51	148.27	5.96
52 (14, 24, 14)	142 (60, 30, 52)	153.77	150.33	6.00

A partial grid refinement study was conducted in an obstructed channel to determine the adequacy of the mesh scheme and to ensure that the solutions are grid independent. Four non-uniform grid sizes were evaluated as shown in Table 1. The computational domain was divided into three parts in both horizontal and vertical directions (see dotted lines in Fig. 1). The left and right parts in the Y-direction are for the width of the obstacles while the middle part in the X-direction is for their length. The data given in parentheses in Table 1 are the number of control volumes used in each part. For example, for the first grid given in Table 1, 10×30 control volumes are used for the obstacles. Each grid is uniform in the horizontal direction and also in the central part in the vertical direction, while non-uniform grids are used for the parts below and above the obstacle in the X-direction. A sine function was chosen as the stretching function with a distribution which concentrated control volumes at the borders.

Differences between the maximum of the stream function Ψ_{max} and the mass flow rate Q for the 42×102 grid (respectively, 42×122) and the finest 52×142 grid were less than 2.5% (respectively 1.5%). For the mean Nusselt number $\overline{Nu}$ the differences were less than one percent for both cases. Based on this study, the 42×102 grid size was used for the simulations.

3. Results and discussion

The computations were performed first for smooth channels to assess the validity of the numerical solutions. Three different aspect ratios were analyzed, $A = 5$, 8, 12, for a channel Rayleigh number range, $10^2 \leqslant Ra^* \leqslant 10^5$. This Rayleigh number is defined as the ratio of the Rayleigh number to the aspect ratio of the channel, i.e. $Ra^* = Ra/A$. All the numerical computations were performed for air ($Pr = 0.71$).

It is well known that for a smooth channel and sufficiently large values of the channel Rayleigh number, i.e. $Ra^* > 10^3$, the mean Nusselt number follows that of the single plate regime (Elenbaas, 1942; Bar-Cohen and Rohsenow, 1984). In Fig. 2, the results of the numerical

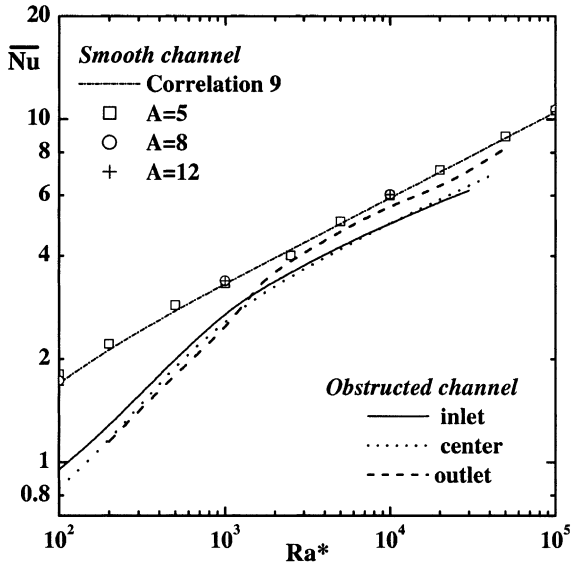

Fig. 2. Variation of the mean Nusselt number versus channel Rayleigh number ($Pr = 0.71$).

simulations for the smooth channel and the correlation of Bar-Cohen and Rohsenow are reported. This correlation, valid for low values of the channel Rayleigh number (fully developed regime) and high values (single plate regime), is as follows:

$$\overline{Nu} = \left[576/Ra^{*2} + 2.873/Ra^{*0.5}\right]^{-0.5}. \quad (9)$$

As can be observed, the points marked by symbols, which represent the numerical simulations for various aspect ratios in the developing flow regime and in the single plate regime, are in good agreement with correlation (9). Thus, this can give us confidence in the numerical simulations reported in what follows.

3.1. Effects of the location of isothermal ribs

Owing to the large number of parameters in this problem, the case with symmetrical isothermal ribs was considered first with a given size of ribs; the width and the length of the ribs are respectively $w^* = 0.3$ and $h^* = 0.2A = 1$. The reduction in the cross-sectional area of the channel is 60%, giving a free flow spacing $a^* = 0.4$ (Fig. 1). These computations were conducted for a channel aspect ratio, $A = 5$. The effects of the ribs were studied at three different locations along the heated wall, designated as the inlet (at $L_1^* = 0.5$), center (at $L_1^* = 2$) and outlet (at $L_1^* = 3.5$) location. From the numerical simulations, the comparisons between the results obtained for an unobstructed channel and those obtained for the channel with obstructions are reported. These results are also compared to those obtained with adiabatic ribs.

Figs. 3 and 4 show the streamlines and isothermal contours at $Ra^* = 1466$ and 2×10^4 for the three different locations of the ribs. For isothermal ribs located near the inlet, the fluid which enters at the ambient temperature is heated efficiently. The temperature difference is near its maximum and the obstacles, acting as an abrupt contraction, greatly disturb the flow. A large recirculation zone downstream of the obstacle increases

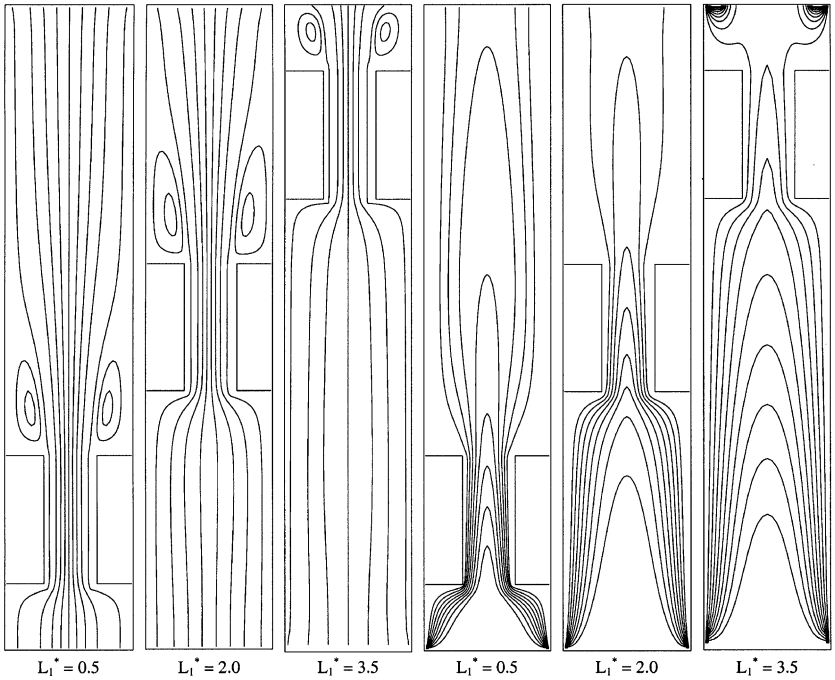

Fig. 3. Streamlines and isothermal contours for three different locations of the ribs ($Ra^* = 1466$, $Pr = 0.71$, $w^* = 0.3$, $h^* = 1$, $A = 5$).

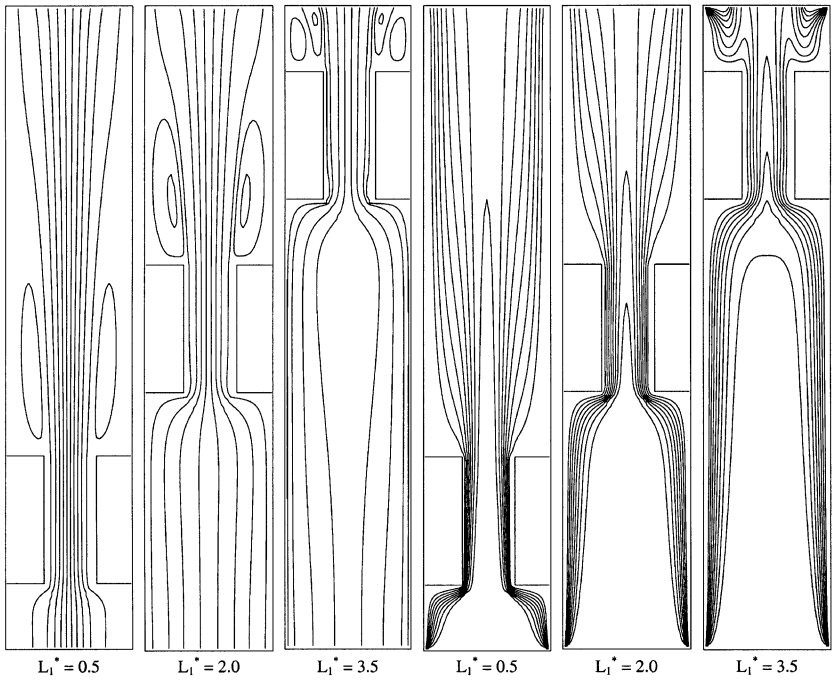

Fig. 4. Streamlines and isothermal contours for three different locations of the ribs ($Ra^* = 2 \times 10^4$, $Pr = 0.71$, $w^* = 0.3$, $h^* = 1$, $A = 5$).

in size when the ribs are moved away from the leading edge of the channel. Increasing the Rayleigh number obviously also strengthens the downstream upper fluid recirculation. It should be noted that in all of the present computations, neither was upstream recirculation flow generated below the horizontal bottom surface of the rib nor was fluid separation detected at the leading edge of the rib along its vertical surface. For outlet ribs, recirculations through the outlet of the channel section occur, supplying ambient fluid inside the channel toward the upper surface of the ribs.

When the flow proceeds downstream, the bulk temperature rises all along the channel, the fluid being heated continuously by the isothermal walls. Thus, the heating efficiency decreases with the temperature difference. As a result, the peak in the local Nusselt number at the obstruction location decreases as L_1^* increases, as can be seen from Figs. 5 and 6, which show the local Nusselt number profiles along the wall for three values of the channel Rayleigh number, 100, 1466 and 2×10^4. It should be noted that the local Nusselt number (Eq. (7)) and the mean Nusselt number (Eq. (8)), are calculated all along the channel wall, i.e. at the base of the rib which acts as an ideal fin in the case of isothermal obstacles. The heat transfer from the horizontal and vertical faces of the ribs is then not explicitly calculated but included in the local value of the Nusselt number along the base of the obstacle. The heat transfer from the bottom of the rib to the fluid is much greater than that extracted from the top due to recirculating flow. As the velocity of the flow increases and reaches its maximum in the restricted area of the channel between the ribs, the local Nusselt number increases sharply. The heat transfer is then maximum at the leading edge of the obstruction, decreases slightly along the vertical surface and reaches a second maximum at the trailing edge of the rib. Beyond the rib, the maximum flow velocity then decreases sharply and the local Nusselt number, whose value is now very low owing to the presence of the downstream vortex, increases before decreasing slowly as the thermal boundary layer grows. For ribs closely located to the outlet of the channel, the downstream recirculation flow goes through the outlet section and ambient fluid is assumed to enter. This is readily seen in Figs. 3 and 4 and, as a consequence, a sharp increase of the heat transfer occurs owing to the ambient fluid, which is supplied through the outlet section (Figs. 5 and 6). It should remembered that the sharp increase is due to incoming air at ambient temperature which is an approximation to the actual situation.

Although these three sets of curves (Figs. 5 and 6) show similar trends, the main features are amplified when the Rayleigh numbers are increased. Owing to the acceleration of the flow in the by-pass region, which is more pronounced at high Rayleigh numbers, the local Nusselt number in this region increases substantially. More important is the strengthening of the vortex with increasing Ra^* which greatly reduces the heat transfer after the rib from the isothermal wall to the main flow. Thus, the local Nusselt number along the recirculation zone is substantially reduced when increasing the Rayleigh number. The local Nusselt number is always close

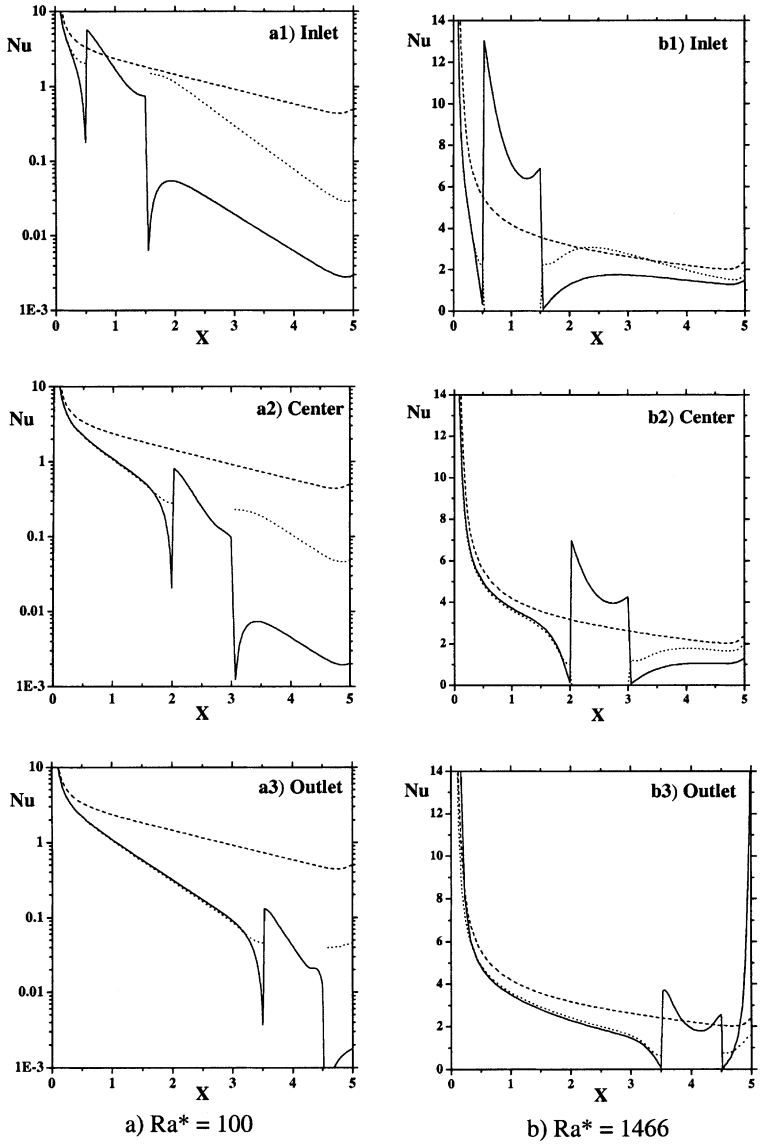

Fig. 5. Comparison of the local Nusselt number profiles for isothermal (full lines) and adiabatic (dotted lines) ribs at two different channel Rayleigh numbers: (a) $Ra^* = 100$ and (b) 1466 ($w^* = 0.3$, $h^* = 1$, $A = 5$, $Pr = 0.71$ (dashed lines: smooth channel)).

to zero at the inside upper rib corner. Lastly, in Fig. 6, the reduced increase in the local Nusselt number for outlet ribs compared to what can be seen in Fig. 5 ($Ra^* = 1466$) comes from the multiple longitudinal rolls appearing over the top surface of the rib through the outlet section at high values of Ra^* (see also Fig. 4). This is also why the second maximum at the trailing edge of the rib is greater than the first at the leading edge.

Fig. 7 shows the variation of the mean Nusselt numbers as a function of the channel Rayleigh number, while the values of the inlet mass flow rate are reported in Fig. 8. For the sake of clarity, the mean *Nu*-curves are also presented in Fig. 2. Moving the obstruction away from the inlet channel towards the channel exit causes a reduction of about 14% in the magnitude of the mean Nusselt number for $Ra^* = 100$, as can be seen in Fig. 7. Flow reversals above the ribs, which strengthen when the obstruction is moved away, explain this behavior. On the other hand, above some critical values of the channel Rayleigh number, the mean Nusselt numbers for the center and outlet ribs become larger compared with that obtained for the inlet location (Fig. 7). This results from the fact that the upper flow reversals, which extend largely downstream after the ribs, inhibit the heat flux from the isothermal wall to the main stream. This trend increases so greatly with Ra^* that only a weak increase of the local Nusselt number beyond the rib appears for $Ra^* = 2 \times 10^4$. The further the location of the rib from the inlet of the channel, the lower the critical Rayleigh number. For the outlet rib, because of the recirculation through the channel outlet supplying ambient fluid, this trend becomes much more marked.

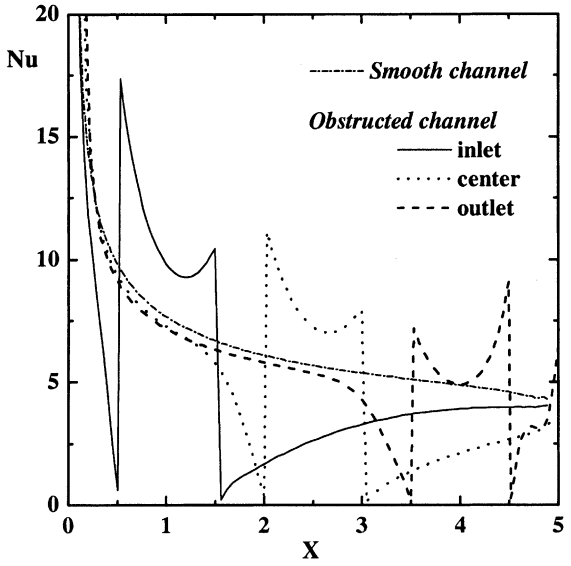

Fig. 6. Local Nusselt number profile along the wall for three different locations of the ribs ($Ra^* = 2 \times 10^4$, $Pr = 0.71$, $w^* = 0.3$, $h^* = 1$, $A = 5$).

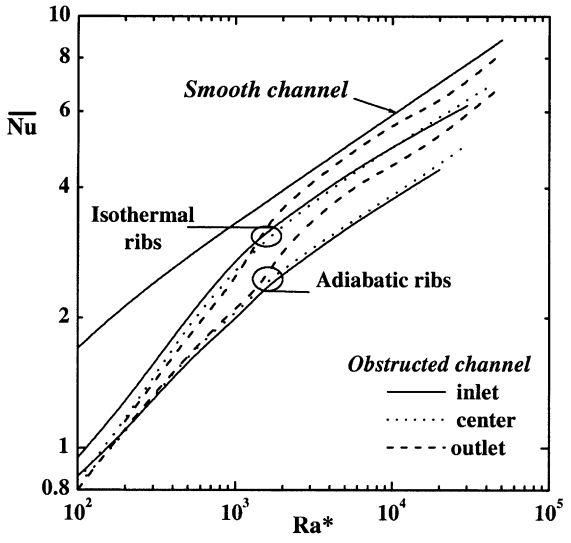

Fig. 7. Variation of the mean Nusselt number versus channel Rayleigh number for obstructed channels ($Pr = 0.71$, $w^* = 0.3$, $h^* = 1$, $A = 5$).

It is obvious that the mean Nusselt numbers are largely below those of a smooth channel, although the heated surface is greater.

As can be observed in Fig. 8 for isothermal ribs, the further the obstruction from the leading edge of the channel, i.e. the greater L_1^*, the lower the inlet flow rate. Clearly, the inlet flow rate of the obstructed channels is significantly lower than that of the unobstructed channel (not presented here, but recall that the free area is only 40%). Increasing the channel Rayleigh number intensifies these trends. While the magnitude of the reduction is almost insignificant at $Ra^* = 100$ when comparing the

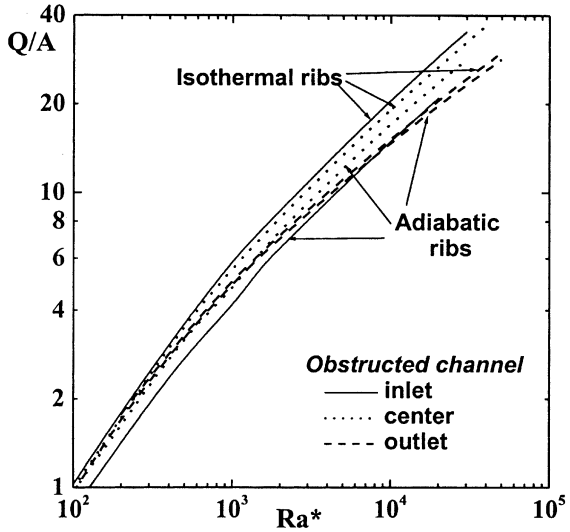

Fig. 8. Variation of the inlet mass flow rate versus channel Rayleigh number for obstructed channels ($Pr = 0.71$, $w^* = 0.3$, $h^* = 1$, $A = 5$).

values of the flow rate for the inlet and outlet ribs, it reaches 15% at $Ra^* = 10^3$ and 26% at $Ra^* = 10^4$. The single plate regime is characterized by two dynamic boundary layers with velocity maximums very close to the walls of the channel. The ribs, which are symmetrically placed on the walls of the channel, are in the path of the boundary layers. The sharp deflections of the stream flows slow down the motion; on the other hand, in the developing flow regime for which the velocity profile is almost parabolic, the velocity is maximum in the center part of the channel and then less perturbed by the ribs. The behavior of the flow at a downstream location—that of the obstruction—influences the mass flow rate at the inlet of the channel by a retroaction effect. At high values of the channel Rayleigh number, the mass flow rate is greater for the inlet than for the outlet position. The length of the channel beyond the obstacles acts as an expanded heated extension; this is the chimney effect (Shahin and Floryan, 1999). Addition of a straight (respectively expanded) chimney at the exit of a channel induces higher flow rates and produces heat transfer enhancements from 10% to 30% (respectively from 30% to 250%). This can be attributed to the pressure loss reaching its maximum near the channel entrance. More ambient air is then pulled inside the channel.

3.2. Effects of the rib thermal conductivity

Very low and very high thermal conductivities are extreme situations between which actual values of the conductivity of the ribs have been and are being studied to give the main trends. For comparison purposes, the variation of the mean Nusselt number versus Ra^* for these three cases, unobstructed channel, obstructed

channel with isothermal and with adiabatic ribs, are also given in Fig. 7. The mean Nusselt number for the three positions of the rib is also given. In the case of adiabatic ribs, the heated surface is smaller not only than that of the obstructed channel with isothermal ribs but also than that of the heated surface of the unobstructed channel. The mean Nusselt number for adiabatic ribs is obviously lower than that in the two other cases. Unexpectedly, the behavior of the Nusselt number in an obstructed channel for isothermal and adiabatic ribs is very similar whatever the location of the obstacle, especially at high values of the channel Rayleigh number. Compared to adiabatic ribs at the center and outlet positions, inlet adiabatic ribs are unfavorable to heat transfer at practically all values of the Rayleigh number. This can be explained by a very large decrease in the inlet flow rate in this case. Referring again to Fig. 8 which shows the inlet flow rate versus the channel Rayleigh number, it can be observed that the gap between the adiabatic and isothermal curves decreases as the ribs are moved away from the channel inlet. The greatest gap is for the inlet rib, and it increases with the Rayleigh number. It seems that an adiabatic contraction situated near the leading edge of a heated channel considerably reduces its flow rate. For the outlet position of the ribs the gap is almost insignificant.

Surprisingly, at low Rayleigh numbers and in the case of center and outlet positions of the obstacle, the mean Nusselt number is of the same order of magnitude for both isothermal and adiabatic obstacles (the relative difference is lower than 2%). Fig. 5 also presents the profile of the local Nusselt number along the heated wall in case of adiabatic ribs for two Rayleigh numbers, $Ra^* = 100$ and 1466. For the isothermal case, a very low value of Nu is reached just before the obstacle, followed by a sharp increase. Beyond the trailing edge, the Nusselt number is once again very weak. This can be observed whatever the Rayleigh number (see also Fig. 6). In the inside lower and upper corners of the obstacle, the merging of the horizontal and vertical boundary layers inhibits the heat transfer from the wall to the flow owing to the hot spot of fluid occurring in these two corners. Moreover, the plume arising from the extended surface of the obstacle, together with the growth of the boundary layer along the wall beyond the obstacle, decrease the heat transfer from the wall. This decrease is greater than that which continuously occurs along a smooth uniformly heated plate. On the other hand, for the adiabatic, case no such sharp decrease can be seen in front of or beyond the obstacle because there is no boundary layer along the extended surface of the obstacle, but only along the heated walls. Furthermore, beyond the adiabatic obstacle, a new boundary layer grows along the wall resulting in better heat transfer compared with isothermal case. At low values of Ra^* this compensates the extended active surface area of the isothermal case and the sharp increase of Nu at the leading edge. With increasing Ra^*, the mass flow rate increases and consequently the heat transfer from the isothermal obstacle sharply increases. The difference between the mean Nusselt numbers in both cases is then clearly distinguishable in Fig. 7, the isothermal case now being more efficient than the adiabatic one. At $Ra^* = 2 \times 10^4$, the relative difference between the Nusselt numbers reaches 20% for centered and outlet ribs.

3.3. Effects of the rib geometry

Two different sets of geometry have been investigated based upon rib length and width from the case previously studied ($w^* = 0.3$, $h^* = 1$, $A = 5$).

The effects of varying the obstacle length are demonstrated by comparing cases with a fixed width, $w^* = 0.3$ (Fig. 9). The greatest effect is for the mean Nusselt number while only slight variations are seen for the mass flow rate. The relative variation of the mass

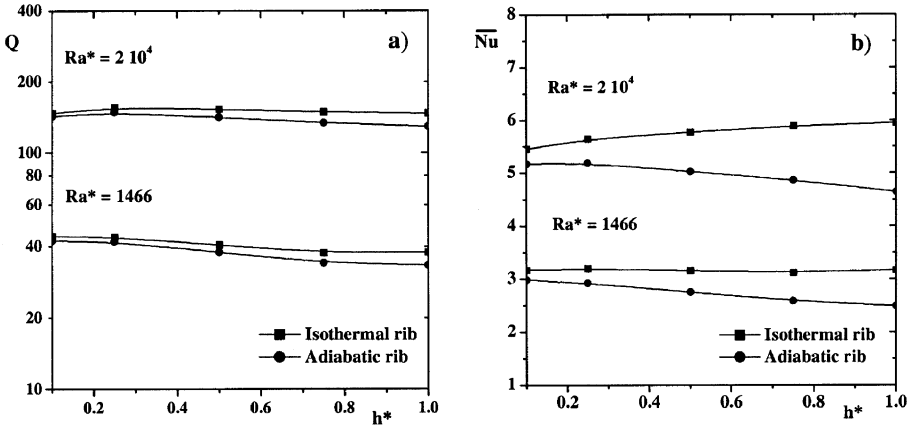

Fig. 9. Variation of the mass flow rate (a) and of the mean Nusselt number (b) in function of the length of the ribs for two different channel Rayleigh numbers ($w^* = 0.3$, $A = 5$, $Pr = 0.71$).

flow rate in the range studied (from $h^* = 0.1$ to 1) is 15% for isothermal ribs at $Ra^* = 1466$ (respectively 7% at $Ra^* = 2 \times 10^4$) and of 22% at $Ra^* = 1466$ (respectively 10%) for adiabatic ribs. The isothermal and adiabatic curves show a similar trend. On the other hand, the mean *Nu*-curves show opposite behaviors. The mean Nusselt number increases only slightly when increasing the length of the isothermal ribs while it decreases for the adiabatic ones. This is clearly because in the first case the heat transfer surface is constant while in the second case it decreases. This trend amplifies when increasing the Rayleigh number. For isothermal ribs and at the lowest value of the Rayleigh number, $Ra^* = 1466$, the mean Nusselt number is almost constant (2% variation) while the relative increase reaches 10% for $Ra^* = 2 \times 10^4$. This is because directly behind the ribs, the main heat transfer mechanism is recirculation, which is only slightly affected by the length of the rib. The increase is essentially due to better heat extraction at the rib coming from fluid flow acceleration, as can be seen in Figs. 5 and 6. For adiabatic ribs, the absolute decreases are almost identical as the rib length increases from 0.1 to 1 whatever the channel Rayleigh number, 0.5 at $Ra^* = 1466$ and 0.53 at $Ra^* = 2 \times 10^2$. In the by-pass region which is adiabatic in this case, the strengthening of the natural convection has obviously no influence on the heat transfer.

Fig. 10 presents the changes in the mass flow rate and in the mean Nusselt number as the rib width increases from 0 to 0.4 for a fixed length of 1. Once again, the values of Q for both cases only differ slightly, showing the same trend, a linear decrease from $w^* = 0$ to 0.25 and a sharp decrease for greatest widths of the rib. This decrease is much greater for the lowest value of the Rayleigh number; from $w^* = 0$ to 0.4, the mass flow rate decreases by a factor of 3 at $Ra^* = 2 \times 10^2$ and a factor of 7 at $Ra^* = 1466$. This can explain the behavior of the mean Nusselt number, which is quite different at the two Rayleigh numbers for the greatest widths of obstruction (i.e., $w^* > 0.3$). At $Ra^* = 2 \times 10^4$, a large difference between the isothermal and adiabatic curves of the Nusselt number appears whatever the rib width. At $Ra^* = 1466$, the curve for the isothermal ribs presents a sharp decrease and the magnitude of the mean Nusselt number at $w^* = 0.4$ is very close to that of the adiabatic ribs. The same kind of phenomenon, exemplified in Fig. 5 ($Ra^* = 100$, centered rib), arises but at a higher value of Ra^* when the width of the rib increases. The effect of the constriction being non-linear beyond $w^* = 0.2$, the mass flow rate is considerably reduced. For isothermal and adiabatic ribs, the heat transfer profiles beyond the rib for $w^* = 0.4$ and $Ra^* = 1466$, are very similar to those presented for $w^* = 0.3$ and $Ra^* = 100$ (Fig. 5). The heat transfer at the rib for the isothermal case is counterbalanced by a better heat extraction beyond the rib in the adiabatic case. This effect only arises for small values of the mean Nusselt number, i.e. close to 1, and is attenuated at higher values of *Nu* for which heat extraction at the rib increases and largely compensates what happens after the rib (see Fig. 5, $Ra^* = 1466$).

3.4. Effects of aspect ratio

The effect of aspect ratio was determined by holding the rib geometry at $w^* = 0.3$, $h^* = 1$ and its location as centered. Extra computations were made for another aspect ratio, $A = 8$, for isothermal and adiabatic ribs. Fig. 11 gives the variations of the mean Nusselt number in both cases and also for $A = 5$. It can be immediately noticed that at low Rayleigh numbers the mean Nusselt number is almost independent of the rib conductivity (see Section 3.1 for an explanation) while the curves diverge as the Rayleigh number increases. At high values of Ra^*, the two isothermal A-curves merge as do the adiabatic ones, indicating that the channel Rayleigh number is always a well-suited dimensionless parameter for the single plate regime (i.e., at high values of Ra^*).

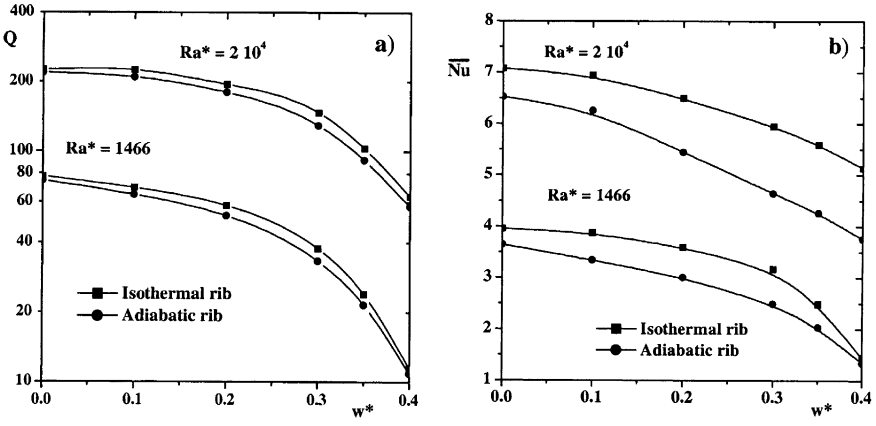

Fig. 10. Variation of the mass flow rate (a) and of the mean Nusselt number (b) as a function fo the width of the ribs for two different channels Rayleigh numbers ($h^* = 1$, $A = 5$, $Pr = 0.71$).

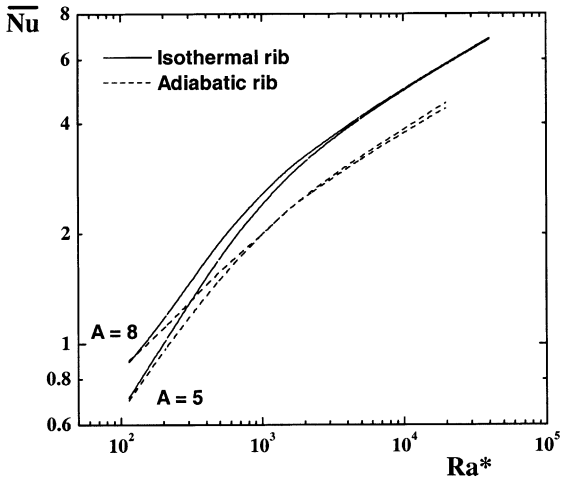

Fig. 11. Variation of the mean Nusselt number in function of the channel Rayleigh number for two different aspect ratios ($w^* = 0.3$, $h^* = 1$, $Pr = 0.71$ (centered ribs)).

4. Conclusions

A numerical study of natural convection in an obstructed vertical channel has been performed. In particular, a channel of aspect ratio 5 with two symmetrical isothermal or adiabatic ribs has been extensively considered. The local and the mean Nusselt numbers and the flow rate as a function of the channel Rayleigh number have been obtained. The results show how, on moving the ribs towards the outlet, the mean Nusselt number increases as the distance of the ribs from the inlet increases, but only for high values of the channel Rayleigh number. The best position of the ribs for heat extraction depends on the magnitude of the Rayleigh number. On the other hand, the inlet flow rate always decreases when the distance of the obstruction from the leading edge of the channel increases, whatever the channel Rayleigh number. It has also been found that the mean Nusselt number behavior at high Rayleigh number is very similar for isothermal and adiabatic ribs whatever their location. The magnitude of the mean Nusselt number is obviously lower for adiabatic obstructions. Finally, it has been shown that increasing the length of the rib has only a limited influence on the heat transfer while increasing its width decreases dramatically the mass flow rate and the heat transfer especially if more than half of the opening is obstructed.

Acknowledgements

The authors acknowledge the help of C. Fischetti with some of the computational work. This work was supported by research grant no. 980715 from the IDRIS-Computer Center (French National Institute for Advances in Scientific Computations). One of the authors (G.D.) is grateful to the Picardie region (Pôle Modélisation) for its financial support.

References

Bar-Cohen, A., Rohsenow, W.M., 1984. Thermally optimum spacing of vertical, natural convection cooled, parallel plates. J. Heat Transfer 116, 116–123.

Bhavnani, S.H., Bergles, A.E., 1990. Effect of surface geometry and orientation on laminar natural convection heat transfer from a vertical flat plate with transverse roughness elements. Int. J. Heat Mass Transfer 33, 965–981.

Bodoia, J.R., Osterle, J.F., 1962. The development of free convection between heated vertical plates. J. Heat Transfer 84, 40–44.

Elenbaas, W., 1942. Heat dissipation of parallel plates by free convection. Physica 9, 1–28.

Habchi, S., Acharya, S., 1986. Laminar mixed convection in a partially blocked, vertical channel. Int. J. Heat Mass Transfer 29, 1711–1722.

Hadjadj, A., Kyal, M., 1999. Effect of two sinusoidal protuberances on natural convection in a vertical concentric annulus. Numer. Heat Transfer 36A, 273–289.

Hung, Y.H., Shiau, W.M., 1988. Local steady-state natural convection heat transfer in vertical parallel plates with a two-dimensional rectangular rib. Int. J. Heat Mass transfer 31, 1279–1288.

Kettleborough, C.F., 1972. Transient laminar free convection between heated vertical plates including entrance effects. Int. J. Heat Mass Transfer 15, 883–896.

Kwak, C.E., Song, T.H., 1998. Experimental and numerical study on natural convection from vertical plates with horizontal rectangular grooves. Int. J. Heat Mass Transfer 41, 2517–2528.

Marcondes, F., Maliska, C.R., 1999. Treatment of the inlet boundary conditions in natural-convection flows in open-ended channels. Numer. Heat Transfer 35B, 317–345.

Nakamura, H., Asako, Y., Naitou, T., 1982. Heat transfer by free convection between two parallel flat plates. Numer. Heat Transfer 5, 95–106.

Patankar, S.V., 1980. Numerical Heat Transfer and Fluid Flow. Hemisphere/McGraw-Hill, Washington.

Said, S.A.M., Krane, R.J., 1990. An analytical and experimental investigation of natural convection heat transfer in vertical channels with a single obstruction. Int. J. Heat Mass Transfer 33, 1121–1134.

Shahin, G.A., Floryan, J.M., 1999. Heat transfer enhancement generated by the chimney effect in systems of vertical channels. J. Heat Transfer 121, 230–232.

Sparrow, E.M., Chrysler, G.M., Azevedo, L.F., 1984. Observed flow reversals and measured-predicted Nusselt numbers for natural convection in a one-sided heated vertical channel. J. Heat Transfer 106, 325–332.

Tanda, G., 1997. Natural convection heat transfer in vertical channels with and without transverse square ribs. Int. J. Heat Mass Transfer 40, 2173–2185.

Zamora, B., Hernandez, J., 1997. Influence of variable property effects on natural convection flows in asymmetrically-heated vertical channels. Int. Comm. Heat Mass Transfer 24, 1153–1162.